Contrib Mineral Petrol (1982) 81:190–202

Contributions to Mineralogy and Petrology

The System Granite-Peridotite-H_2O at 30 kbar, with Applications to Hybridization in Subduction Zone Magmatism

T. Sekine* and P.J. Wyllie
Department of the Geophysical Sciences, University of Chicago, Chicago, Illinois 60637, USA

Abstract. Experiments with mixtures of granite, peridotite and H_2O at 30 kbar were designed as a first step to test the hypothesis that the calc-alkaline igneous rocks of subduction zones are formed by differentiation of magmas derived by partial melting of hybrid rocks generated in the mantle wedge, by reaction between hydrous siliceous magma rising from subducted oceanic crust, and the overlying mantle peridotite. Experiments were conducted in gold capsules in half-inch diameter piston-cylinder apparatus. Results are presented in a 900° C isotherm, and in a projection of vapor-present phase fields onto T-granite-peridotite. Isobaric solution of peridotite in hydrous, H_2O-undersaturated granite liquid at 900° C causes only small changes in liquid composition, followed by precipitation of orthopyroxene until about half of the liquid has solidified; then orthopyroxene is joined by jadeitic clinopyroxene, garnet, and phlogopite. Phlogopite-garnet-websterite continues to be precipitated, with evolution of aqueous vapor, until all of the liquid is used up. The product of hybridization is a pyroxenite without olivine. The products of partial melting of this material would differ from products derived from peridotite because there is no olivine control, and the clinopyroxenes contain up to 7% Na_2O, compared with less than 1% Na_2O in peridotite clinopyroxenes. The reaction products are directly analogous to those in the model system $KAlSiO_4-Mg_2SiO_4-SiO_2-H_2O$, where, with decreasing SiO_2 in the hydrous siliceous liquid, the field for phlogopite expands, and phlogopite instead of orthopyroxene becomes the primary mineral. If this occurs with less siliceous magmas from the subducted oceanic crust, there is a prospect for separation of discrete bodies of phlogopite-rock as well as phlogopite-garnet-websterite. We need to know the products of hybridization, and the products of partial melting of the hybrid rocks through a range of conditions.

Introduction

The first experiments aimed at the petrology of subduction zones supported the idea that andesites could be primary magmas from subducted oceanic crust (Green and Ringwood 1968; Green 1972). Allen et al. (1975) and Allen and Boettcher (1978) presented experimental results for amphibolites supporting this view. Experimental studies by Kushiro (1972) and Mysen and Boettcher (1975) indicating that andesites could be primary magmas derived from mantle peridotite flushed by aqueous fluids rising from the subducted slab were denied by the experiments of Nicholls (1974) and Green (1976). Current interpretations of experimental and geochemical data favor complex multisource processes (e.g. Green 1980; Wyllie 1981).

At the end of his comprehensive review on andesites, Gill (1981, p. 315) concluded that: "few orogenic andesites are unfractionated primary melts. Most are derivative, the residues of low pressure fractionation." He continued: "The parent melts are hybrid basalts which contain contributions from both the chemically heterogeneous mantle wedge and subducted oceanic crust", and he concluded that the proportions of various components and the details of differentiation remain speculations, constituting "the chief andesite problems for the 1980's".

One process involving both subducted oceanic crust and the overlying mantle is the hybridization scheme proposed by Nicholls and Ringwood (1973). They suggested that hydrous siliceous melts resembling rhyodacites in composition were generated in the oceanic crust, and then reacted with the overlying peridotite. They proposed that the magmas would produce hybrid zones of olivine pyroxenite immediately above the oceanic slab, at depths of 100–150 km. Diapirs would rise episodically from this zone, and subsequent partial melting of these wet, hybrid rocks would produce a wide range of calc-alkaline magmas, which may differentiate before eruption. There are very few experimental data on the interactions among hydrothermal fluids, magmas, and rocks at high pressures, and no direct experimental tests on the products of hybridization between hydrous siliceous melts and peridotite.

One way to investigate the products of hybridization is to model the phase relationships in synthetic silicate systems. Sekine and Wyllie (1982a) explored the data available in a system which includes representatives of (1) hydrous siliceous magma from subducted oceanic crust – the eutectic liquid in the system $KAlSi_3O_8-SiO_2-H_2O$, and (2) the overlying mantle – the assemblage forsterite + enstatite in the system $Mg_2SiO_4-SiO_2-H_2O$. They extended their exploration in a series of systems with one additional component, $NaAlSiO_4$, $CaMgSi_2O_6$, $CaAl_2Si_2O_8$, and Al_2O_3 (Sekine and Wyllie, 1982b).

* *Present address:* Department of Earth Sciences, Monash University, Clayton, Victoria 3168, Australia.

0010-7999/82/0081/0190/$02.60

Hybridization is not a simple mixing process, because of the incongruent melting of phlogopite and of enstatite. The products of hybridization in the system $KAlSiO_4-Mg_2SiO_4-SiO_2-H_2O$, under suitable physical conditions, could lead to the concentration of potassium from the liquid into deposits of phlogopite or phlogopite + enstatite. It appears from the more complex systems that this conclusion could be extended to the assemblage phlogopite + orthopyroxene + clinopyroxene (with jadeite in solid solution), but the critical phase equilibrium data delineating the extent of the liquidus field for phlogopite in relationship to the other minerals are not available.

Another approach to the problem is to take whole-rock samples as starting materials. This approach involves too many components for graphical representation in standard phase diagrams. In this contribution, we investigate the phase fields intersected by mixtures of a natural granite and a natural peridotite, in the presence of H_2O, at 30 kbar pressure corresponding to a depth of about 100 km. From the results, we can select the products that might be produced if hydrous siliceous melt mixes with crystalline peridotite, using the processes deduced in the synthetic systems as a guide to the mixture of natural rock systems.

Starting Materials

The starting materials were natural rocks with known geology, mineralogy, chemistry, and phase relationships. The samples were ground to pass 200-mesh sieve, dried, mixed, and stored in a desiccator. The powders were composed for the most part of very small grains, with larger grains of most minerals averaging 30 microns, rarely ranging up to 70 microns in longest dimension.

Granite

The chemical composition and norm of the biotite granite from the Sierra Nevada Batholith are given in Table 1. The sample was kindly provided by P.C. Bateman and F.C. Dodge for phase equilibrium studies. Reviews of the geology, mineralogy and petrology have been cited in Piwinskii (1968a) and Stern and Wyllie (1981). The volumetric mode of the sample is: quartz, 34.8%; potassic feldspar, 29.0%; plagioclase, 31.5%; mafic minerals (mainly biotite), 4.7%.

The phase relationships for this sample have been determined to 35 kbar with variable amounts of H_2O. Selected phase boundaries relevant to the present study at 30 kbar are reproduced in Fig. 1.

Figure 1A shows the effect of high pressure on the mineralogy of granite, the effect of excess H_2O on the melting-crystallization interval of granite, and the H_2O-undersaturated liquidus surface, extending to the dry liquidus. The 30 kbar section through the liquidus and solidus of granite in the presence of H_2O is shown in Fig. 1B, together with the mineral assemblages coexisting with liquid between these boundaries.

The most directly applicable mixing experiments would use not granite, but a composition corresponding to that of the magma escaping from subducted oceanic basalt. However, the compositions of near-solidus liquids from quartz-eclogite have so far defied experimental determination or calculation (Stern and Wyllie 1978; Sekine et al. 1981). Nicholls and Ringwood (1973) suggested that they resembled rhyodacite, which is not too dissimilar from granite. There are two advantages to using granite in these experiments: (1) the behavior of potassium can be followed more readily with granite than with some other composition with low potassium selected to approximate more closely the probable composition of the actual magma, and (2) it would take some years to determine the phase relationships of the probable magma, even if its composition were known, whereas the phase relationships of the granite are already known in detail. It is desirable to determine the range of compositions of minerals produced in mixing reactions as a function of composition of introduced siliceous melt and, also, to determine the compositions of melts that can be derived from the hybrid material.

Table 1. Chemical compositions and CIPW norms of the starting materials

	1	2	M_1	M_2	M_3	M_4
SiO_2	42.22	75.4	72.4	66.3	60.6	52.8
TiO_2	0.30	0.15	0.17	0.20	0.23	0.28
Al_2O_3	4.42	13.5	12.6	10.9	9.25	7.01
Cr_2O_3	0.50	–	0.05	0.16	0.25	0.39
Fe_2O_3	2.86	0.0	0.30	0.91	1.46	2.23
FeO	4.45	0.64	1.05	1.86	2.61	3.65
MnO	0.13	0.04	0.05	0.07	0.09	0.11
NiO	0.27	–	0.03	0.09	0.14	0.21
MgO	34.61	0.10	3.76	11.08	17.75	27.08
CaO	3.92	1.0	1.32	1.95	2.52	3.33
Na_2O	0.43	4.0	3.65	2.94	2.29	1.39
K_2O	0.11	4.6	4.15	3.26	2.44	1.30
H_2O^+	5.73	0.35	0.31	0.25	0.18	0.09
H_2O^-	0.19	0.04	–	–	–	–
P_2O_5	0.05	0.07	0.06	0.06	0.06	0.06
Cl	0.20	–	–	–	0.10	0.15
CO_2	–	0.05	–	–	–	–
Total	100.39	99.94	99.90	100.03	99.97	100.08
$\frac{100Mg}{Mg+\Sigma Fe}$	89.8	21.9	83.5	88.1	89.0	89.5
CIPW norm						
Qz	–	31.6	26.1	15.5	5.7	–
Or	0.72	27.2	24.5	19.3	14.4	7.7
Ab	3.88	34.1	30.9	24.9	19.4	11.7
An	10.37	5.0	5.8	6.8	7.8	9.1
Di	7.77	–	0.6	2.3	3.4	5.6
Hy	17.74	0.6	10.9	29.0	46.0	41.8
Ol	53.60	–	–	–	–	19.5
Mt	4.40	–	0.5	1.3	2.1	3.2
Il	0.61	0.3	0.3	0.4	0.4	0.5
Cr	0.78	–	–	0.3	0.4	0.6
Ap	0.12	–	–	–	0.1	0.1

1 St. Paul's periodotite mylonite (18–900), Melson et al. (1967), Melson et al. (1972)
2 Biotite granite (104) from the Sierra Nevada batholith
M_1 Mixture of 90 wt% No. 2 granite and 10 wt% garnet peridotite recrystallized from No. 1
M_2 Mixture of 70 wt% No. 2 granite and 30 wt% garnet peridotite recrystallized from No. 1
M_3 Mixture of 51.8 wt% No. 2 granite and 48.2 wt% No. 1 peridotite (anhydrous)
M_4 Mixture of 26.3 wt% No. 2 granite and 73.7 wt% No. 1 peridotite (anhydrous)

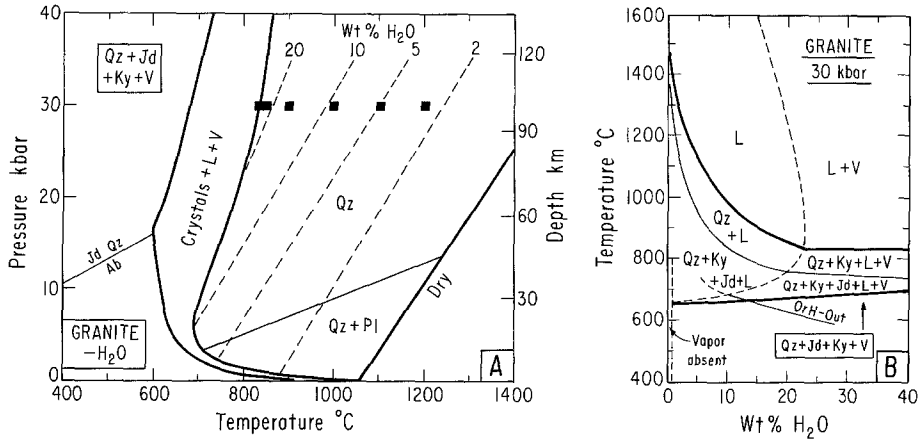

Fig. 1. Selected phase relationships for the biotite-granite of Dinkey Lakes, Sierra Nevada (Table 1), from a series of investigations beginning with Piwinskii (1968b), and collated and reviewed by Stern and Wyllie (1981). A. Results for excess vapor, and the H_2O-undersaturated liquidus surface. The positions of runs conducted with mixtures are shown (Table 4). B. $T-X_{H_2O}$ section at 30 kbar. *Abbreviations: Ab,* albite; *Jd,* jadeite; *Qz,* quartz, or polymorphs of SiO_2; *Ky,* kyanite; *Pl,* plagioclase; *OrH,* orthoclase hydrate; *L,* liquid; *V,* vapor

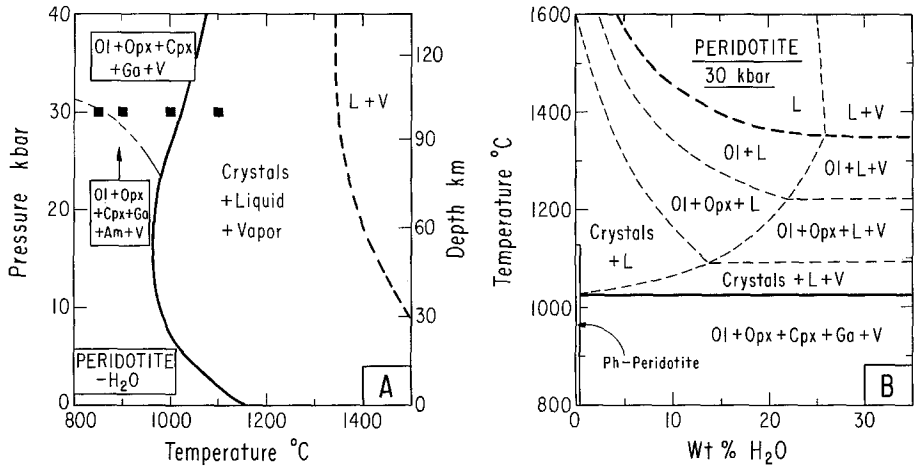

Fig. 2. Selected and estimated phase relationships for the mantle-derived peridotite mylonite from St. Paul's Rocks (Table 1). A. Results for excess vapor, based on experiments of Millhollen et al. (1974) with 5.7% H_2O. The subsolidus mineralogy at 30 kbar was confirmed by the run points plotted (Table 2). B. Schematic $T-X_{H_2O}$ section at 30 kbar. *Abbreviations: Ol,* olivine; *Opx,* orthopyroxene; *Cpx,* clinopyroxene; *Ga,* garnet; *Am,* amphibole; *Ph,* phlogopite; *L,* liquid; *V,* vapor

Peridotite

The chemical composition and norm of the partially hydrated peridotite mylonite from St. Paul's Rocks are given in Table 1. This is a mantle-derived peridotite according to detailed accounts of mineralogy and petrology by Melson et al. (1967; 1972) and Frey (1970). Our sample (kindly supplied by W.G. Melson) is pargasite-rich spinel peridotite mylonite. An X-ray diffraction pattern revealed amphibole, olivine and serpentine, but no pyroxenes. Minor chromian spinel and a trace of orthopyroxene were detected optically.

The phase relationships for this sample, containing 5.7% H_2O in hydrous minerals, were determined by Millhollen et al. (1974) up to 30 kbar, with microprobe analyses reported by Nehru and Wyllie (1975). Figure 2A shows the effect of high pressure on the mineralogy of the peridotite, the effect of H_2O on the solidus, and a rough estimate of the effect of excess H_2O on the liquidus (compare Fig. 1A). The 30 kbar section shown in Fig. 2B is an estimate of the effect of H_2O on the phase fields between liquidus and solidus, based on excess H_2O results, and by analogy with the pattern of phase relationships in Fig. 1A and similar diagrams. The presence of phlogopite has not been reported in experiments on this peridotite, but at 30 kbar the small amount of K_2O in the rock could generate a trace of phlogopite in vapor-absent peridotite (Green 1973). The results of Ryabchikov and Boettcher (1980) indicate that the K_2O would dissolve in the presence of free vapor.

Peridotite-Granite-H_2O Mixtures

The compositions of four mixtures prepared from the crystalline granite (G) and peridotite are listed in Table 1 and plotted in Fig. 3 as M_1, M_2, M_3, and M_4 (the mixtures 90G10P, 70G30P, 51.8G48.2P, and 26.3G73.7P, respectively). M_3 and M_4 were made using the crystalline peridotite (P). M_1 and M_2 were made using garnet peridotite prepared by recrystallizing peridotite P at 30 kbar (see Fig. 2A and Table 2). The CIPW norms of these mixtures are listed in Table 1. Note the abundance of normative hypersthene and orthoclase, and that normative olivine occurs only in mixture M_4. Runs were made with known proportions of H_2O added to the mixtures, as plotted in Fig. 3.

As a framework for selection and interpretation of runs, Fig. 3 also shows the estimated positions of field boundaries for the H_2O-saturated liquidus, and for the coexisting vaporus boundary. The liquidus boundary, L(xls,V), connects the two H_2O-saturated liquidus points in Figs. 1B and 2B (Wyllie 1979, Fig. 18). The vaporus boundary, V(xls,L) is even less well established. The estimate of the vapor composition coexisting with peridotite is based on the results of Ryabchikov et al. (1982) in the sytem $Mg_2SiO_4-SiO_2-H_2O$. The much higher estimate for the solubility of granite in aqueous vapor is based on the results of Ryabchikow et al. (1982) demonstrating a marked increase in solute solubility with increase in SiO_2/MgO (see also the solubility curve for albite in H_2O to 10 kb in Wyllie 1979, Fig. 18). These two field boundaries delineate the

Table 2. Experimental results on peridotite with 5.7% H_2O at 30 kbar

Run #	Temp (°C)	Hours	Phases identified
P-1	1,100	22	Ol + Opx + Cpx + Ga + Gl
P-2	1,000	43	Ol + Opx + Cpx + Ga + Rt(?)
P-3	900	99	Ol + Opx + Cpx + Ga + Rt
P-4	850	120	Ol + Opx + Cpx + Ga + Am + Rt

Abbreviations: Ol, olivine; *Opx,* orthopyroxene; *Cpx,* clinopyroxene; *Ga,* garnet; *Gl,* glass (quenched liquid); *Am,* amphibole; *Rt,* rutile; (?), suspected

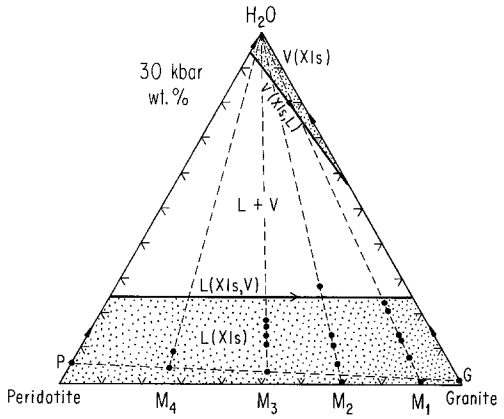

Fig. 3. Compositions of mixtures, M_1–M_4, used in experiments, with H_2O added. M_3 and M_4 were made with the natural, hydrated peridotite, and M_1 and M_2 were made with the recrystallized peridotite (Table 1). The shaded areas are the estimated H_2O-undersaturated liquidus surface, and the subsolidus vaporus surface, each limited by the specified field boundary. *Abbreviations: xls,* crystals; *L,* liquid; *V,* vapor

shaded areas for the H_2O-undersaturated liquidus surface, and the subsolidus vaporus surface.

Experimental Methods

The crushed samples were sealed with water into gold capsules, and reacted at 30 kbar in half-inch diameter piston-cylinder apparatus, using a piston-in procedure with furnace assemblies made of NaCl. No correction was required for friction, and pressures are believed accurate to ±5%. Thermocouples used were calibrated W5%Re/W26%Re, with temperatures precise to ±5° C, and maximum error ±15° C (Huang and Wyllie 1975). Loss of iron from sample to capsule was not a problem, because temperatures of runs were low enough for the use of gold rather than platinum or palladium (Merrill and Wyllie 1973; Nehru and Wyllie 1975). The oxygen fugacity in the capsule is somewhat lower than that corresponding to the hematite-magnetite buffer (Personal communication, R. Altherr 1980).

Run products were examined by optical microscope, X-ray diffraction, and electron microprobe. Analyses of the minerals and glasses were determined by ARL-EMX electron microprobe with energy-dispersive X-ray detector and the data reduction program by Reed and Ware (1973). The analytical system was checked by standards before measuring samples. In general, the accuracy is considered to be within ±2% relative for element concentrations greater than 5%, and ±5% relative for concentrations less than 5%. The analysis of hydrous glasses is subject to special problems. The glass samples were moved by hand during most analyses, for counting times of 60 seconds, in order to reduce volatilization of alkalis by the electron beam.

Mineralogy of Peridotite at 30 kbar

For petrogenetic interpretations, we need to compare the mineralogy of the hybridization products with that of the peridotite. Millhollen et al. (1974) determined the phase relationships of this peridotite to 30 kbar, and Nehru and Wyllie (1975) measured compositions of Ol, Opx, Cpx, and Am produced subsolidus at 20 kbar. We conducted several experiments to establish the subsolidus mineral compositions at 30 kbar. The run conditions are plotted in Fig. 1A, and the results are listed in Table 2, with mineral analyses given in Table 3, and illustrated in Fig. 4A. Figure 4B compares other results obtained for peridotites and model peridotite systems at 30 kbar.

The crushed, crystalline peridotite (containing 5.7% H_2O in minerals, Table 1) was reacted in gold capsules for longer run durations than those of most previous experiments with natural peridotites. The products of all four runs between 850° C and 1,100° C included Ol + Opx + Cpx + Ga. The run at 1,100° C contained a small amount of glass and some orthopyroxene crystals surrounded by thin rims of clinopyroxene. The other three runs contained a trace of rutile. The run at 850° C contained amphibole in addition, approximately equal in amount to the clinopyroxene.

The amphibole-out curve in Fig. 2A was extrapolated to between 850° C and 900° C at 30 kbar from data presented by Millhollen et al. (1974), who were unable to reverse the breakdown of amphibole near 27 kbar. Mysen and Boettcher (1975), working with higher concentrations of vapor, determined the subsolidus amphibole-out curve in peridotites to be at pressures below 25 kbar. Green (1973) placed it close to 30 kbar with 6% H_2O present.

The analytical results for the run at 850° C given in Table 3, and plotted in Fig. 4A, confirm that equilibrium was not achieved with only 5.7% H_2O in a run of 120 h duration. The composition of most of the amphibole analyzed was similar to the pargasite in the original peridotite, but divergent results (Table 3) may represent the partial breakdown products associated with the formation of garnet and clinopyroxene. The garnets analyzed from the 850° C run occupied two groups, one characterized by low CaO and Al_2O_3 and high MgO and SiO_2, and the other with these values reversed and with high TiO_2. The clinopyroxenes were too small for satisfactory analyses.

In the temperature range 850° C to 1,100° C, Mg/(Mg + Fe*) varied from 0.91–0.93 for olivine. Equilibrium was not reached at 850° C, but the compositions of the four major minerals produced at 900° C, 1,000° C and 1,100° C showed little compositional variation within each run (see standard deviations in Table 3). The compositions of garnet and pyroxenes coexisting with olivine at each temperature (except 850° C) are compared in Fig. 4A. Values of Mg/(Mg + Fe*) for orthopyroxene and clinopyroxene are 0.92 and 0.93, respectively. With decreasing temperature, CaO and Al_2O_3 decrease in orthopyroxene, and Al_2O_3 (adjusted for Na_2O and Cr_2O_3) decreases in clinopyroxene. Na_2O

Table 3. Compositions of olivines, orthopyroxenes, clinopyroxenes, garnets, and amphiboles in the peridotite recrystallized at 30 kbar, determined by microprobe

Run #	P-1				P-2				Am[b]
Temp. (°C)	1,100				1,000				
Phase	Ol	Opx	Cpx	Ga	Ol	Opx	Cpx	Ga	
n	7	7	6	3	7	7	5	7	
SiO_2	41.0 (39)	55.7 (46)	53.3 (46)	41.5 (55)	41.9 (1.06)	56.9 (38)	53.5 (26)	43.0 (61)	46.1
TiO_2	–	–	0.00	0.13 (22)	–	–	0.00	0.35 (17)	0.2
Al_2O_3	–	3.51 (68)	2.98 (35)	20.1 (60)	–	1.98 (36)	2.23 (21)	21.4 (90)	11.8
Cr_2O_3	–	0.59 (16)	0.96 (23)	3.63 (39)	–	–	0.42 (42)	0.99 (33)	–
FeO[a]	7.95 (43)	5.02 (42)	2.63 (28)	6.28 (39)	9.25 (33)	5.81 (25)	2.43 (19)	7.79 (19)	4.0
MgO	50.1 (43)	33.2 (47)	18.3 (47)	19.2 (18)	50.3 (79)	35.0 (44)	18.3 (40)	21.5 (1.24)	20.4
CaO	0.0	0.98 (15)	20.6 (25)	7.39 (74)	0.00	0.67 (09)	21.7 (45)	6.34 (47)	11.6
Na_2O	–	0.00	0.47 (43)	0.00	–	–	0.44 (09)	0.00	2.5
K_2O	–	–	–	–	–	–	–	–	0.2
Total	99.05	99.00	99.24	98.23	101.40	100.36	99.02	101.37	96.8
mole prop.									
100 Mg/Mg+ΣFe[a]	91.8	92.2	92.5	84.5	90.7	91.5	93.1	83.1	90.0
Ca	0.0	1.9	42.9	19.0	0.0	1.2	44.2	15.0	26.9
Mg	91.8	90.4	52.9	68.4	90.7	90.3	51.9	70.7	65.8
Fe	8.2	7.7	4.3	12.6	9.3	8.4	3.9	14.4	7.2

Run #	P-3				P-4					
Temp. (°C)	900				850					
Phase	Ol	Opx	Cpx	Ga	Ol	Ga		Am		
n	7	6	4	9	5	5	2	5	1	3
SiO_2	41.3 (49)	56.7 (1.44)	53.1 (50)	41.9 (53)	40.9 (39)	43.3	41.0	46.0	45.7	49.0
TiO_2	–	0.00	0.00	0.40 (47)	–	0.46	1.38	0.83	0.57	0.36
Al_2O_3	–	1.79 (57)	2.74 (58)	21.8 (1.11)	–	20.6	22.1	12.3	11.1	8.85
Cr_2O_3	–	0.00	0.46 (57)	0.84 (47)	–	0.62	0.53	0.12	0.90	0.59
FeO[a]	8.90 (39)	5.64 (36)	2.34 (58)	8.22 (49)	9.15 (39)	8.39	7.51	3.91	4.62	2.87
MgO	49.4 (52)	35.9 (1.01)	18.5 (1.84)	18.5 (71)	49.9 (27)	20.0	16.0	19.8	23.3	20.5
CaO	0.00	0.41 (12)	21.8 (93)	7.21 (61)	0.04 (10)	8.19	12.4	12.0	8.66	12.5
Na_2O	–	–	1.08 (33)	0.00	–	0.00	0.00	3.42	3.27	3.49
K_2O	–	–	0.00	0.00	–	–	–	0.26	0.20	0.19
Total	99.60	100.44	100.02	98.87	99.99	101.56	101.92	98.64	98.32	98.35
mole prop.										
100 Mg/Mg+Fe[a]	90.8	91.9	93.4	80.0	90.7	81.0	79.2	90.0	90.0	92.7
Ca	0.0	0.8	44.1	18.3	0.0	19.2	30.5	28.2	19.4	29.0
Mg	90.8	91.2	52.2	65.4	90.7	65.4	55.0	64.6	72.6	65.9
Fe	9.2	8.0	3.7	16.3	9.3	15.4	14.5	7.2	8.1	5.2

Abbreviations: see Table 2; *n*, number of analyzed points; ( ), standard deviations

[a] FeO = total Fe as FeO

[b] Average pargasite augen in sample 18–900 (Melson et al. 1972)

content of clinopyroxene varies between 0.44 and 1.08. The garnet from the 1,000° C run has higher (MgO + FeO)/CaO than those from runs at 900° C and 1,100° C, but there is progressive increase in FeO* content with decreasing temperature.

Other results for analyzed minerals from peridotites crystallized at 30–31 kbar and 1,100° C are plotted for comparison in Fig. 4B. Mori and Green (1978) presented data from 950–1,100° C and 30–40 kbar which are generally consistent with data of Akella (1976) from 1,100–1,300° C and 31–44 kbar, although Akella's garnet composition is displaced from the other garnet points in the same sense as that for 1,000° C in Fig. 4A. A possible explanation is oxidation of iron, with some of the Fe* substituting as Fe^{3+} for Al^{3+}.

The compositions of pyroxenes and garnets measured in the synthetic model systems $CaO-MgO-SiO_2$ and $CaO-MgO-Al_2O_3-SiO_2$ at 900° C, 1,000° C, and

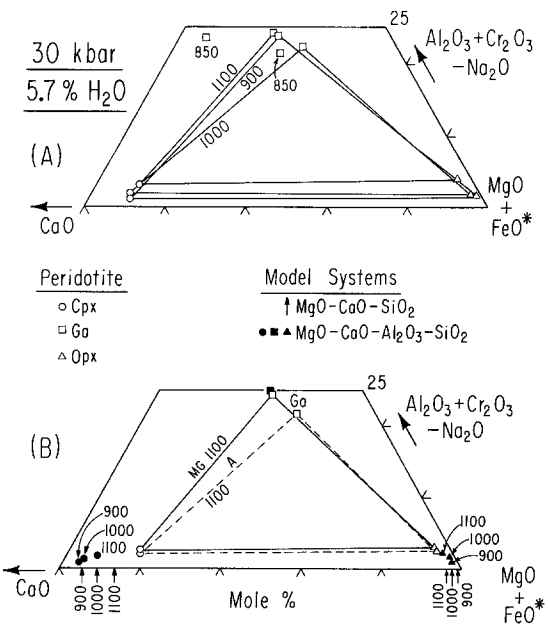

Fig. 4. **A** Compositions of orthopyroxenes, clinopyroxenes, and garnets in peridotite recrystallized at 30 kb, and various temperatures (Table 3). **B** Compositions of minerals from experimentally recrystallized peridotite according to Akella (1976) and Mori and Green (1978), and from model systems CaO – MgO – SiO_2 (Nehru and Wyllie 1974; Lindsley and Dixon 1976; Perkins and Newton 1980) and CaO – MgO – Al_2O_3 – SiO_2 (Perkins and Newton 1980)

1,100° C are given in Fig. 4B. The values of coexisting pyroxenes have been carefully reversed for use in geothermometry and geobarometry (Perkins and Newton 1980), but the difference between pyroxene compositions in the model systems and those determined in the complex peridotite systems confirms the need for caution in application of the model system results to natural peridotites. The largest discrepancies are for clinopyroxene compositions, with those in Fig. 4B diverging more from the model compositions than our results in Fig. 4A. The compositions of garnets in both model and peridotite systems concentrate around grossular 16 ± 2 mole per cent.

Experimental Results for Peridotite-Granite-H_2O at 30 kbar

Experimental results are listed in Table 4. All runs were conducted at temperatures above the H_2O-saturated liquidus of granite, as shown by the points in Fig. 1A, but the starting mixtures plotted in Fig. 3 show that with one exception, they contained less than saturation levels of H_2O.

Phase Relationships

The results are illustrated in a 900° C isotherm (Fig. 5), and in Fig. 6. Figure 6 is a T-peridotite-granite projection of vapor-present phase fields, based on both vapor-present and vapor-absent runs.

At 900° C, peridotite is subsolidus for all H_2O contents (Figs. 2 and 5), and granite is (1) above the liquidus with sufficient H_2O, or (2) consists of crystals + liquid for low

Table 4. Experimental results on mixtures of granite and peridotite with H_2O at 30 kbar

Run #	Temp. (°C)	Hours	wt% H_2O	Phases identified
Composition M_1: 10 wt% recrystallized garnet peridotite + 90 wt% granite				
GP-1	1,000	48	12.6	Opx + Gl(95%)[a]
GP-3	900	93	17.2	Opx + Gl(90%)
GP-7	900	120	7.7	Opx + Cpx + Ga + Qz + Gl(65%)
GP-5	850	120	20.4	Opx + Cpx + Ga(?) + Gl(70%)
GP-6	830	233	22.4	Opx + Cpx + Ga + Ph + Qz + Gl(70%)
Composition M_2: 30 wt% recrystallized garnet peridotite + 70 wt% granite				
GP-2	1,000	48	10.9	Opx + Gl(75%)
GP-9	900	74	27.8	Opx + Gl(50%) + V
GP-4	900	93	13.4	Opx + Ga(tr) + Gl(15%)
GP-8	900	120	5.6	Opx + Cpx + Ph + Qz + Gl(10%)
Composition M_3: 48.2 wt% peridotite + 51.8 wt% granite				
GP-14	1,200	3	15.8	Opx + Gl(60%) + V
GP-18	1,100	8	13.2	Opx + Gl(40%)
GP-15A	1,000	49	12.1	Opx + Cpx + Ga + Ph(?) + Gl(15%) + V
GP-20	900	91	17.5	Opx + Cpx + Ga + Ph + Gl(5%) + V
GP-16	900	95	11.0	Opx + Cpx + Ga + Ph + Gl(5%)
GP-19	900	91	2.8	Opx + Cpx + Ga + Ph + Qz + Gl(?)
GP-21	830	233	12.1	Opx + Cpx + Ga + Ph + Gl(?) + V
Composition M_4: 73.7 wt% peridotite + 26.3 wt% granite				
GP-13	1,100	7	8.8	Opx + Ga + Ph + Gl(40%)
GP-10	1,000	47	8.3	Opx + Cpx + Ga + Ph + Gl(10%)
GP-11	900	93	8.2	Opx + Cpx + Ga + Ph + V

Abbreviations: Ph, phlogopite; *Qz*, polymorphs of SiO_2; *V*, vapor; *tr*, trace; and for others see Table 2

[a] Figures in parentheses give approximate amounts of glasses in run products

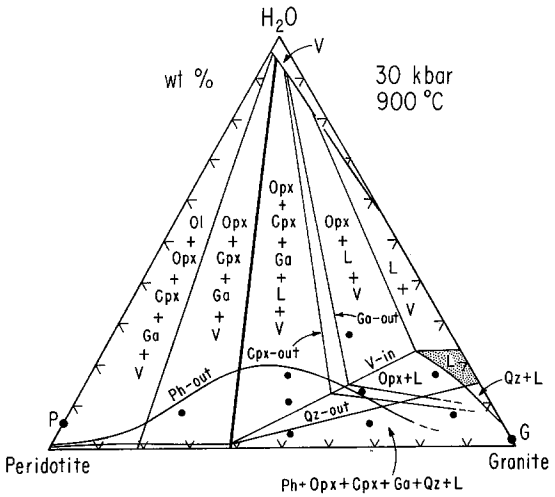

Fig. 5. Isobaric isothermal section through peridotite-granite-H_2O based on Fig. 1B and 2B, runs in Table 4, and other data and estimates given in text. Compare Fig. 3. Note the heavy line for the solidus. *Abbreviations:* see Figs. 1 and 2

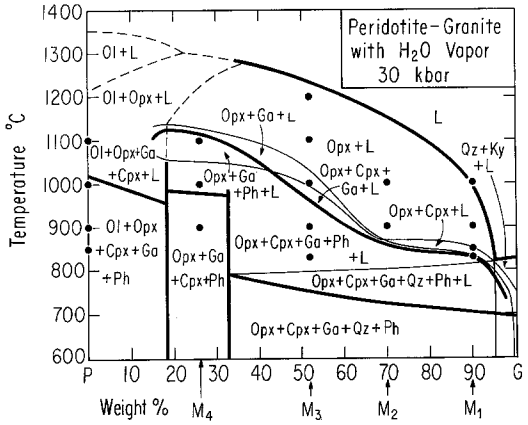

Fig. 6. Phase fields with a small amount of vapor in system peridotite-granite-H_2O, constructed as described in text. Compare Fig. 5 for 900° C supplementary diagram. Complex subliquidus and subsolidus phase assemblages near granite are omitted (see Fig. 1B). Note the subsolidus field for phlogopite-garnet-websterite separating fields with olivine and quartz. Note the upper stability limit for phlogopite. *Abbreviations:* see Figs. 1 and 2

H_2O contents (Figs. 1 and 5). For the peridotite-granite system at 900° C, phase assemblages with liquid occupy an area extending from granite-H_2O to the solidus line, which connects a composition near 40G60P to the aqueous vapor.

The subsolidus phase assemblages with vapor consist of garnet-peridotite or garnet-pyroxenite, with a trace of phlogopite for low H_2O contents. The results of Ryabchikov and Boettcher (1980) on the solubility of phlogopite in aqueous vapor at high pressures were used in addition to the runs to estimate the position of the phlogopite-out curve in Fig. 5. There is also a line barely separated from the anhydrous base giving the H_2O-content of vapor-absent phlogopite-pyroxenite and phlogopite-peridotite (Fig. 2B).

For the phase assemblages with liquid on the right-hand side of the solidus line, the vapor-in boundary extends from a point near the anhydrous base at the solidus, to the H_2O-saturated liquid line, with about 25% H_2O. Figure 5 shows that with addition of peridotite, the L+V field on the join granite-H_2O is replaced successively by vapor-present fields with Opx+L, pyroxenes+L, and garnet pyroxenite+L. Phlogopite occurs in the last two assemblages for H_2O contents below the Ph-out curve. With decreasing H_2O in the vapor-absent region, these phase assemblages are joined by quartz. The quartz-out curve extends from the granite-H_2O join (Figs. 1B and 5) to the solidus line near the anhydrous base (Fig. 5). Phlogopite stability reaches its maximum range for mixtures intermediate between peridotite and granite, because it needs components from both rocks.

Figure 6 illustrates the distribution of the major phase volumes containing a small amount of vapor, based on runs with excess vapor, vapor-absent runs, and isothermal sections such as Fig. 5. Although few of the phase boundaries are closely defined by vapor-present runs, the distribution of phase volumes is unambiguous. The diagram is divided into three parts by the two vertical lines, corresponding to the boundaries in Fig. 5 separating olivine-bearing assemblages from pyroxenite, and subsolidus pyroxenite from partially melted pyroxenite. These three parts are occupied by subsolidus garnet-peridotite, garnet-pyroxenite, and quartz-garnet-pyroxenite. For each rock in the presence of H_2O there is a different solidus, with varying temperature caused by solid solutions in the mafic minerals. There are complex adjustments near granite as the phase assemblage is reduced to Qz+Jd+Ky+V (Fig. 1B), but these need not concern us.

The runs demonstrate that between the field for olivine extending from peridotite-H_2O (Fig. 2B), and the field for quartz extending from granite-H_2O (Fig. 1B), the liquidus is dominated by orthopyroxene. The orthopyroxene liquidus rises steeply from the low-temperature liquidus piercing point for L(Opx,Qz,V) near the granite-H_2O side. The field for Opx+L+V extends through 200° C or more below the liquidus, to a series of contiguous boundaries for clinopyroxene, garnet, and phlogopite, which brings in an extensive phase field for phlogopite-garnet-pyroxenite with L+V. Quartz is added to the assemblage below about 800° C. Table 4 lists the estimated percentage of glass from partially melted runs.

Glass Compositions

The problems of analyzing alkali contents of hydrous glasses with electron microprobe are well-known. For example, Kushiro (1974) compared analyses for H_2O-saturated glasses quenched from 15 kbar in the system Fo–An–Qz obtained by using broad and sharp electron beams, with liquid compositions determined by phase assemblage geometry. Na_2O contents were lower in the microprobe analyses, and reduced even further with the sharp beam (2 μm). There was no significant difference in SiO_2, Al_2O_3, CaO, and MgO contents by the different methods.

The glass compositions listed in Table 5 determined with the sample moving continuously under the electron beam during analysis for 60 s are compared with spot analyses for 60 s. The surface of the sample was not visibly changed after the first type of analysis, but a hole was burned in the surface during spot analyses. The differences between the raw totals and 100% in Table 5, ranging from 14–20%,

Table 5. Compositions of hydrous glasses, quenched at 30 kbar, measured by microprobe, and recalculated to 100%

Starting composition	Original granite	90G10P(M_1)						70G30P(M_2)					51.8G48.2P(M_3)		
Run #		GP-1	GP-3		GP-7	GP-5	GP-6	GP-2	GP-9	GP-4		GP-8	GP-15A	GP-20	GP-16
Temp (°C)		1,000	900	S	900	850	830	1,000	900	900	S	900	1,000	900 S	900 S
SiO_2	76.0	75.9	75.6	78.4	78.1	74.3	77.4	76.5	76.1	73.3	76.3	74.2	74.7	75.1	77.2
Al_2O_3	13.6	12.9	13.1	14.0	15.6	13.4	13.7	14.6	13.6	14.3	15.7	14.9	16.6	15.8	15.8
FeO*	0.64	0.7	0.75	0.0	0.0	0.5	0.0	0.6	0.0	0.4	0.0	0.8	0.0	0.0	0.0
MgO	0.1	1.7	1.6	0.85	0.6	1.3	1.2	1.4	0.7	1.5	0.5	2.0	1.0	1.3	0.8
CaO	1.0	1.25	1.15	1.21	0.0	0.1	1.1	2.8	2.25	2.1	2.1	0.7	1.5	1.7	0.9
Na_2O	4.0	3.3	3.25	2.4	1.9	6.5	2.9	1.3	3.5	3.7	1.95	3.5	2.8	3.1	2.5
K_2O	4.6	4.35	4.50	3.2	3.8	3.9	3.8	2.8	3.8	4.7	3.4	4.0	3.4	3.0	2.9
Raw Total		85.8	86.1	83.2	85.1	82.6	85.8	79.6	80.0	81.3	80.1	87.6	83.6	85.3	85.6
Difference from 100%		14.2	13.9	16.8	14.9	17.4	14.2	20.4	20.0	18.7	19.9	12.4	16.4	14.7	14.4
$\frac{100\,Mg}{Mg+\Sigma Fe^*}$	22	81	80	100	100	83	100	80	100	87	100	82	100	100	100

S = spot analysis for 60 seconds

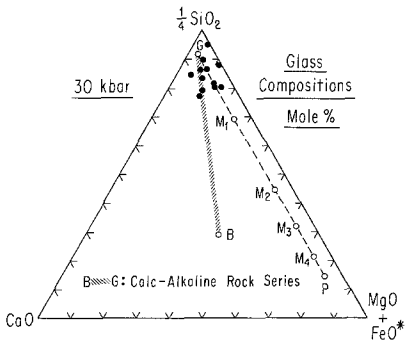

Fig. 7. Compositions of glasses (Table 5) from runs in Table 4, projected into diagram for comparison with the starting mixtures (line PG) and with the average chemical variation of the calc-alkaline igneous series (BG)

represent the minimum H_2O dissolved in the liquid during a run. The anhydrous analyses have been recalculated to 100% in Table 5. For the spot analyses, values of SiO_2 and Al_2O_3 are higher, and those of FeO*, MgO, Na_2O, and K_2O are lower than values measured by the moving analyses. There is no difference in CaO contents. The raw totals by spot analysis are lower by 1–3%. The values of 100 Mg/(Mg + Fe*) vary between 80 and 87, except for glasses with negligible amounts of FeO*.

Glass analyses from Table 5 are plotted in Fig. 7, and compared with the four starting mixtures on the mixing line P–G, and with the average chemical variation of the calc-alkaline igneous series, B–A–D–R (Stern and Wyllie 1978; Sekine et al. 1981). All glasses measured in phase assemblages from mixtures M_3, M_2, and M_1 have compositions clustered towards the original granite, indicating that solution of the peridotite components in the liquid was limited. We could detect no systematic variations in alkalis

Table 6. Compositions of clinopyroxenes

Starting composition	M_1 90G10P		M_2 70G30P	M_3 51.8G48.2P					M_4 26.3G73.7P	
Run #	GP-7	GP-5	GP-8	GP-15A	GP-20	GP-16	GP-19	GP-21	GP-10	GP-11
Temp. (°C)	900	850	900	1,000	900	900	900	830	1,000	900
n	8	6	5	1	3	2	3	3	1	4
SiO_2	56.4	55.3	57.7	53.8	53.8	54.9	56.2	55.7	54.1	54.2
Al_2O_3	14.6	8.78	14.4	4.15	4.49	8.24	10.8	8.00	3.92	5.14
Cr_2O_3	0.0	0.91	0.0	0.57	0.27	1.90	0.0	0.0	0.0	0.34
FeO*	3.39	3.48	2.74	2.65	2.60	2.41	2.17	2.06	2.19	2.61
MgO	10.2	11.3	10.0	16.6	16.1	12.4	13.0	13.0	16.2	16.3
CaO	7.74	14.1	6.42	19.5	19.5	15.3	12.3	15.6	20.1	19.6
Na_2O	7.35	5.12	7.82	1.78	1.79	4.12	4.78	3.90	1.64	2.56
Total	99.68	98.99	99.08	99.05	98.55	99.27	99.25	98.26	98.15	100.75

n = number of analyzed points

Table 7. Compositions of Orthopyroxenes

Starting composition	M_1 90G10P						M_2 70G30P				
Run #	GP-1	GP-3	GP-7	GP-5		GP-6	GP-2	GP-9	GP-4	GP-8	
Temp. (°C)	1,000	900	900	850		830	1,000	900	900	900	
n	3	6	3	3	3	4	4	4	5	5	6
SiO_2	56.1	57.2	57.0	56.3	56.1	58.1	56.7	57.2	55.3	57.3	58.0
Al_2O_3	3.31	2.89	2.11	1.64	2.39	3.20	2.58	2.53	2.58	2.22	3.78
FeO*	7.85	10.2	9.27	11.1	6.63	6.19	6.52	5.70	7.23	6.27	7.19
MgO	31.0	31.1	32.6	30.5	33.6	33.7	32.5	33.6	32.9	33.9	30.9
CaO	0.33	0.38	0.22	0.44	0.50	0.59	0.46	0.45	0.52	0.33	0.43
Total	98.60	101.77	101.20	99.98	99.22	101.78	98.76	99.48	98.53	100.02	100.30

Starting composition	M_3 51.8G48.2P							M_4 26.3G73.7P		
Run #	GP-14	GP-18	GP-15A	GP-20	GP-16	GP-19	GP-21	GP-13	GP-10	GP-11
Temp. °C	1,200	1,100	1,000	900	900	900	830	1,100	1,000	900
n	5	4	5	8	4	2	4	4	4	3
SiO_2	58.2	58.1	56.8	47.0	57.3	58.0	56.9	57.3	57.3	57.7
Al_2O_3	2.68	3.27	4.09	3.54	3.53	4.69	3.59	4.09	2.94	2.79
FeO*	4.40	5.31	6.31	6.74	6.83	6.11	7.23	5.46	5.74	6.27
MgO	35.6	33.8	32.8	33.2	32.9	30.4	32.8	34.3	34.0	34.3
CaO	0.50	0.70	0.78	0.69	0.49	0.41	0.48	0.83	0.63	0.19
Total	101.38	101.18	100.78	101.17	101.05	99.61	101.00	101.98	100.61	101.25

n = number of analyzed points

or other elements as a function of mixture composition or temperature.

Compositions of Pyroxenes

Orthopyroxenes and clinopyroxenes in the runs from mixtures grew larger and formed stouter prisms than those in the recrystallized peridotite. Orthopyroxenes grew to 15–20 × 35–40 μm, and clinopyroxenes to 25 × 30 μm. Their compositions are given in Tables 6 and 7. Clinopyroxenes from the run products and recrystallized peridotite are plotted in Fig. 8, and both pyroxenes are compared with garnet compositions and the mineralogy of peridotite in Fig. 9. The values of Mg/(Mg+Fe*) for Opx and Cpx are lower than those of the starting mixtures (Table 1), and lower than those in recrystallized peridotite at corresponding temperature (Table 3). The lowest values are for orthopyroxenes from mixture M_1.

Figure 8 shows the composition points for clinopyroxenes from each run, which are averaged in Table 6. Cr_2O_3 contents are variable. All clinopyroxenes from the mixtures are enriched in Na_2O and Al_2O_3 compared with clinopyroxene in the peridotite, the increases for runs with M_1 and M_2 being much greater than for runs with M_3 and M_4. Calculation of formulae based on 6 oxygens indicates that most of the Na in these runs is fixed by jadeite, but Al is distributed between jadeite and Ca-Tschermak's molecule. The variation of Na_2O in Fig. 8 is thus equivalent to variation in jadeite component.

Examination of Fig. 8 with details of the runs in Table 4

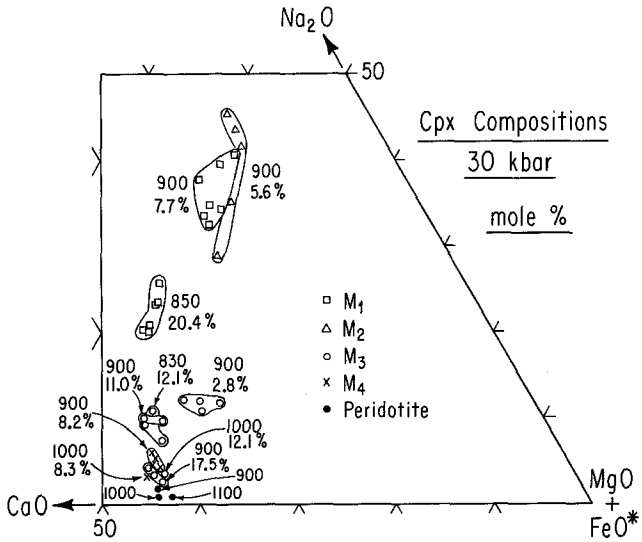

Fig. 8. Compositions of clinopyroxenes (Table 6) from runs in Table 4, for comparison of Na_2O contents of hybrid, jadeitic clinopyroxenes with those in recrystallized peridotite (Tables 2 and 3). Temperatures and weight % H_2O are listed

and the isotherm in Fig. 5 reveals the following trends. The jadeite content of the clinopyroxene varies as a function of temperature, H_2O content, and bulk composition of the solid starting mixture. For a given bulk composition and H_2O content, the jadeite component changes very little from 830–900° C (M_3 with 12.1–11.0% H_2O), but it decreases with temperature increase from 900–1,000° C (M_3

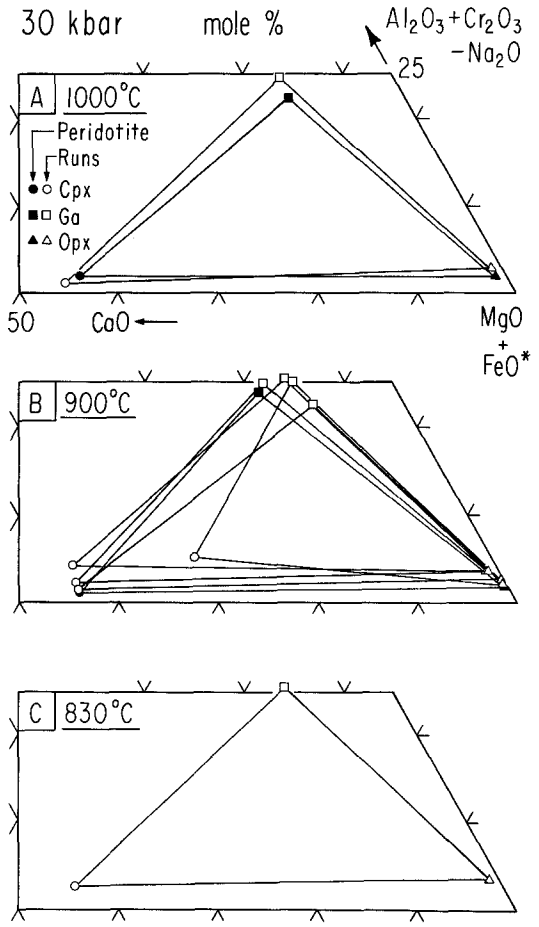

Fig. 9. The compositions of garnet and pyroxenes from the mixed runs at various temperatures (Tables 4, 6, 7 and 8), compared with those of recrystallized peridotite (Tables 2 and 3)

with 11.0–12.1% H_2O, and M_4 with 8.2–8.3% H_2O). For a given mixture composition and temperature (or small temperature range), the jadeite component decreases with increasing H_2O content (M_1, 850–900° C, 7.7–20.4% H_2O; M_3, 900° C, 2.8–11.0–17.5% H_2O). For given temperature and H_2O content (or within limited ranges of these), the jadeite component decreases with increasing peridotite component in the mixture, from M_1 to M_3 to M_4. (M_1–M_3, 850–900° C with 20.4–17.5% H_2O, and 900° C with 7.7–11.0% H_2O; M_1–M_4, 900° C with 7.7–8.2% H_2O; M_3–M_4, 900° C with 11.0–8.2% H_2O). The one set of analyses from M_2 occupies about the same compositional range as those from M_1 under similar conditions (900° C, 5.6–7.7% H_2O).

The clinopyroxenes with the highest jadeite components are those from runs on mixtures M_1, M_2, and GP-19 from M_3. These runs contained no vapor phase. The dashed line separates these results from most runs with M_3 and M_4, which contained vapor. Change in bulk composition toward granite, with increasing Na_2O and Al_2O_3, should cause enrichment of clinopyroxene in jadeite, but the jadeite content could possibly be reduced in the presence of a vapor phase capable of dissolving high quantities of the solid components (see Figs. 3 and 5).

Figure 9 reproduces from Fig. 4A the compositions of coexisting garnet and pyroxenes from peridotite recrystallized at 1,000° C and 900° C, for comparison with analyses of the corresponding assemblages produced in Figs. 5 and 6, and Table 4. Most of the points for clinopyroxene, recalculated from Table 6, contain more Al_2O_3 than the peridotite clinopyroxene, despite the compensation for jadeite in the projection, indicating the presence of Ca-Tschermak's molecule. The clinopyroxene in Fig. 9B differing from all others represents the 12 analyses with highest Na_2O (and lowest CaO) in Fig. 8, from M_1 and M_2 (runs GP-7 and GP-8 in Table 6).

Orthopyroxene analyses are listed in Table 7. The points plotted in Fig. 9 have somewhat higher $Al_2O_3+Cr_2O_3-Na_2O$ than those in the peridotite. Variations in CaO and Al_2O_3 and MgO/(MgO+FeO*) revealed no consistent trends as a function of temperature and bulk composition of mixture.

Compositions of Garnets

Garnet analyses are listed in Table 8. Most of the garnets lie close to the stoichiometric join $(Al_2O_3+Cr_2O_3-Al_2O_3)=25$ (Fig. 9), except for that which coexists with the jadeite-rich clinopyroxene from M_1 at 900° C (run GP-7).

Table 8. Compositions of garnets

Starting composition	M_1 90G10P	M_3 51.8G48.2P			M_4 26.3G73.7P		
Run #	GP-7	GP-20	GP-16	GP-21	GP-13	GP-10	GP-11
Temp. (°C)	900	900	900	830	1,100	1,000	900
n	3	6	4	2	3	5	6
SiO_2	42.1	41.9	42.3	41.7	42.4	41.7	42.9
TiO_2	0.0	0.0	0.0	0.30	0.0	0.36	0.30
Al_2O_3	23.3	23.1	24.0	23.8	23.1	23.1	21.2
Cr_2O_3	0.65	1.21	0.53	0.16	1.48	0.56	0.43
FeO*	11.0	9.10	9.44	10.6	6.63	8.19	9.00
MnO	0.32	0.0	0.0	0.39	0.0	0.0	0.19
MgO	17.9	18.3	19.0	17.6	20.3	19.5	20.6
CaO	5.18	6.89	5.72	5.58	6.51	6.10	5.01
Total	100.45	100.50	100.99	100.13	100.42	99.51	99.54

n = number of analyzed points

Table 9. Compositions of phlogopites

Starting composition	M_1 90G10P	M_3 51.8G48.2P				M_4 26.3G73.7P		
Run #	GP-6	GP-20	GP-16	GP-19	GP-21	GP-13	GP-10	GP-11
Temp. °C	830	900	900	900	830	1,100	1,000	900
n	4	1	1	4	4	3	1	3
SiO_2	45.2	42.5	44.6	43.8	43.3	41.0	41.3	42.0
TiO_2	1.1	1.01	1.48	2.37	1.04	0.44	0.98	0.84
Al_2O_3	16.3	14.9	16.3	17.4	15.5	15.6	15.7	15.9
Cr_2O_3	0.0	0.56	0.0	1.57	0.20	0.33	0.0	0.0
FeO*	3.81	2.87	3.00	2.90	2.96	3.54	3.18	2.91
MgO	20.6	22.5	20.8	17.5	21.6	24.2	23.8	25.0
CaO	0.0	0.0	0.33	0.0	0.0	0.22	0.28	0.10
Na_2O	0.0	0.50	0.0	0.56	0.69	0.44	1.09	0.61
K_2O	9.56	9.28	9.63	9.72	9.41	9.66	9.14	8.64
Total	96.65	94.12	96.14	95.82	94.70	95.43	95.47	96.00

n = number of analyzed points

Compositions of Phlogopites

The analyses listed in Table 9 confirm that the micas produced in the runs are phlogopite, with high MgO/FeO* and K_2O/Na_2O.

Products of Mixing Hydrous Granite Liquid with Peridotite

Figure 10 shows some of the phase fields from the isothermal section at 900° C in Fig. 5. Consider H_2O-undersaturated granite liquid L at 900° C and 30 kbar. If this is emplaced within peridotite and allowed to reach equilibrium at constant pressure and temperature, the bulk composition of the mixing system would change along the line L–P.

Solution of peridotite components would cause the liquid composition to change along L–A. With continued reaction, orthopyroxene is precipitated as the bulk composition changes along A–B, and the liquid composition departs from the composition plane. With continued reaction, several changes occur. Orthopyroxene is joined by clinopyroxene, garnet, and phlogopite, and aqueous vapor is evolved, as the bulk composition changes from B to C. During the interval from C to D, the remaining liquid continues to precipitate phlogopite-garnet-pyroxenite, with evolution of aqueous vapor, until the last liquid is used up at the solidus, D. Throughout this process, the liquid composition remains rich in SiO_2, and close to the general area L–A, as shown by analyses in Table 5 and Fig. 7. The effect of adding peridotite to the siliceous magma is to cause precipitation of cafemic minerals, with the Na_2O and K_2O from the liquid being transferred to jadeite component in clinopyroxene (Table 6, Fig. 8) and to phlogopite (Table 9), respectively. The final product is a body of phlogopite-garnet-websterite, with mineral compositions differing from those in the host peridotite, especially with respect to the clinopyroxene.

The vapor-present part of the line L–P in Fig. 10 can be viewed at 900° C in Fig. 6. The sequence of products described for 900° C remains essentially the same for temperatures between about 850° C and 1,000° C. At lower temperatures, it requires less peridotite to bring about precipitation of clinopyroxene, garnet, and phlogopite along with the orthopyroxene. Note in Fig. 6 the curve limiting the precipitation of phlogopite.

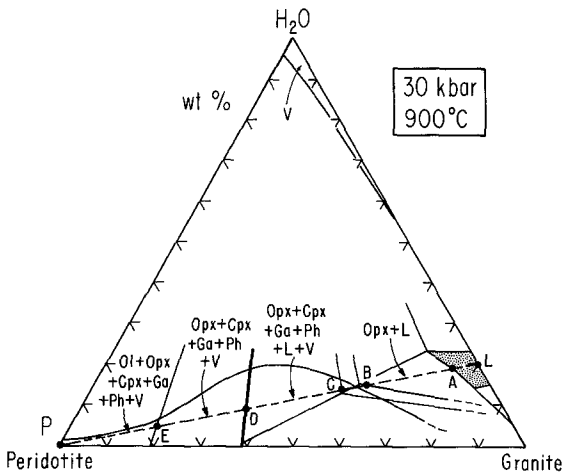

Fig. 10. Products of mixing hydrous, H_2O-undersaturated siliceous liquid, L, with subsolidus peridotite, P, under isothermal, isobaric conditions. Compare Fig. 5. The reaction product is phlogopite-garnet-websterite and vapor, with bulk composition D, and jadeitic clinopyroxene (Fig. 8). The liquid composition to the end remains siliceous, near A (Fig. 7). *Abbreviations:* see Figs. 1 and 2

The mixing products in the system granite-peridotite-H_2O are directly analogous to those described in the model system $KAlSiO_4-Mg_2SiO_4-SiO_2-H_2O$ by Sekine and Wyllie (1982a, Fig. 4). The join Ph–En in the model system serves the same function as a mineral-precipitation barrier between the low-temperature, hydrous siliceous liquid and the subsolidus peridotite as does the subsolidus interval for phlogopite-garnet-websterite in the rock system (Fig. 6). In the model system, specific liquid paths can be traced, illustrating how the liquid is constrained to remain rich in SiO_2 while the minerals are precipitated by reaction with the peridotite components. Furthermore, different T-composition slices can be sketched for the model system, illustrating how the effect of SiO_2 content of the siliceous liquid affects the distribution of the phase fields intersected by joins anal-

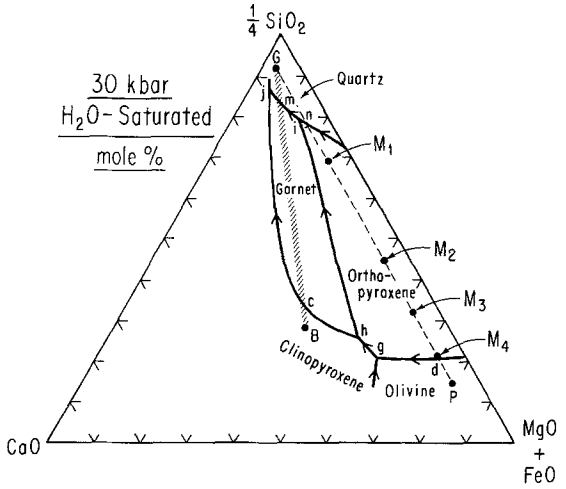

Fig. 11. Pseudoternary field boundaries for excess H_2O, separating areas for the primary crystallization of minerals, based on experiments with calc-alkaline rock series, BG (from Stern and Wyllie 1978, Fig. 15), and with mixtures between peridotite and granite, PG (Figs. 5 and 6, and Table 4)

ogous to Fig. 6. Sekine and Wyllie (1982a, Fig. 5) showed that for decreasing SiO_2 in the original liquid corresponding to L in Fig. 5, the field of Ph+L expands relative to that of En+L, and phlogopite becomes the primary mineral of the steep liquidus rising from the low-temperature piercing point. This suggests that for a natural system with peridotite and a magma less siliceous than granite rising from the subducted oceanic crust, Fig. 6 would be modified in a similar way, with the curve limiting the crystallization of phlogopite moving to the right, and approaching or reaching the liquidus.

Hybridization of Magma Rising from Subducted Slab into Peridotite

Wyllie and Sekine (1982) extrapolated results from the model system to complex rock compositions, and discussed the products generated above the subducted oceanic crust by hybridization of cool, hydrous magmas escaping from the crust into the hotter, overlying peridotite. They concluded that the products would be a series of discrete masses composed largely of phlogopite, orthopyroxene, and clinopyroxene (enriched in jadeite). The results in Figs. 5 and 6 confirm the formation of this assemblage, with garnet as an additional mineral.

In the model system, quartz (or coesite) can be generated along with phlogopite at low temperatures for some mixing lines. For granite-peridotite, the field for partially melted quartz-pyroxenites is limited to low H_2O contents (Fig. 5) as well as low temperatures (Fig. 10), and there appears to be less chance that quartz would be included among the hybrid products in the natural rock systems.

Wyllie and Sekine (1982) reviewed the implications of the hybridization process for magma generation in subduction zones, according to the extrapolated results from the model system. The results described in this paper support the conclusions reached in that published review.

Phase Relationships, Rock Series, and Rock Mixtures

Figure 11 incorporates pseudoternary phase relationships presented by Stern and Wyllie (1978, Fig. 15) with Fig. 7 of this paper, and extends the phase relationships according to the experimental results in Figs. 5 and 6. Stern and Wyllie (1978) emphasized that the lines separating primary phase fields on this triangle were in reality neither ternary phase boundaries nor lines, but they serve a useful purpose in delineating visually the relative positions of primary liquidus minerals, and liquid paths projected from hyperdimensional space.

Stern and Wyllie (1978) determined the phase relationships for a series of natural rocks (basalt-andesite-rhyolite) in the presence of H_2O, and on the basis of these results they presented a pseudoternary diagram with boundaries connecting *c, j,* and *m* in Fig. 11. The boundaries separate fields for the primary crystallization of clinopyroxene, garnet, and quartz, and relate these fields to the composition line for the rock series (B–G in Fig. 11). Figure 11 shows in addition the mixing line between peridotite-granite (P-G) studied in this investigation (Fig. 7).

Figure 6 shows that there is an extensive field for primary orthopyroxene extending across the composition join P-G, with fields for primary olivine and quartz at either end. In Fig. 11, these fields have been linked with those delineated by Stern and Wyllie (1978) by adding a field boundary *hi* for L(Ga,Opx), and a short field boundary *gh* for L(Opx,Cpx), which is the liquidus expression of the subsolidus assemblage for pyroxenite without olivine or quartz in Fig. 6.

Stern and Wyllie (1978) concluded that liquids generated by the partial fusion of subducted oceanic crust at depths of 100 km or so would be controlled by the hyperdimensional equivalent of boundary *jc* for L(Ga,Cpx) in Fig. 11, and would therefore have CaO/(MgO + FeO) higher than the average values of the calc-alkaline igneous series. This conclusion was supported by analogous experiments in the model system $CaO-MgO-Al_2O_3-SiO_2-H_2O$ by Sekine et al. (1981).

The hydrous siliceous melts rising into peridotite from subducted oceanic crust are represented by liquids on the field boundary near *j*, L(Cpx,Ga,Qz). We have demonstrated that emplacement of liquids with composition G in Fig. 11 produces liquids with compositions limited to the region *jmin* (Fig. 7). The liquids remain siliceous until completely solidified, and do not reach compositions corresponding to those of the average calc-alkaline igenous rocks. Further experiments are required to explore the hybridization products between peridotite and less siliceous liquids, corresponding to those changing composition along a path such as *jc* in Fig. 11. Once we have a better knowledge of magma compositions generated in subducted oceanic slabs, and the degree of partial melting (and thus composition) required for upward escape, we will be in a better position to select the most definitive melt compositions for elucidation of this problem. Then, we need to determine the products of partial melting of the hybrid products through a range of conditions.

Acknowledgments. This research was supported by the Earth Sciences Section of the National Science Foundation, NSF Grant EAR 81-08626.

References

Akella J (1976) Garnet pyroxene equilibria in the system $CaSiO_3-MgSiO_3-Al_2O_3$ and in a natural mineral mixture. Am Mineral 61:589–598

Allen JC, Boettcher AL (1978) Amphiboles in andesite and basalt: II. Stability as a function of $P-T-f_{H_2O}-f_{O_2}$. Am Mineral 63:1074–1087

Allen JC, Boettcher AL, Marland G (1975) Amphiboles in andesite and basalt: I. Stability as a function of $P-T-f_{O_2}$. Am Mineral 60:1069–1085

Frey FA (1970) Rare earth and potassium abundances in St. Paul's rocks. Earth Planet Sci Lett 7:351–360

Gill JB (1981) Orogenic andesites and plate tectonics. Springer-Verlag, New York, p 390

Green DH (1973) Experimental melting studies on a model upper mantle composition at high pressure under water-saturated and water-undersaturated conditions. Earth Planet Sci Lett 19:37–53

Green DH (1976) Experimental testing of "equilibrium" partial melting of peridotite under water-saturated, high-pressure conditions. Can Mineral 14:255–268

Green TH (1972) Crystallization of calc-alkaline andesite under controlled high-pressure hydrous conditions. Contrib Mineral Petrol 34:150–166

Green TH (1980) Island arc and continent building magmatism – a review of petrogenic models based on experimental petrology and geochemistry. Tectonophysics 63:367–385

Green TH, Ringwood AE (1968) Genesis of calc-alkaline igneous rock suite. Contrib Mineral Petrol 18:105–162

Huang W-L, Wyllie PJ (1975) Melting reactions in the system $NaAlSi_3O_8-KAlSi_3O_8-SiO_2$ to 35 kilobars, dry and with excess water. J Geol 83:737–748

Kushiro I (1972) Effect of water on composition of magmas formed at high pressures. J Petrol 13:311–334

Kushiro I (1974) Melting of hydrous upper mantle and possible generation of andesitic magma: an approach from synthetic systems. Earth Planet Sci Lett 22:294–299

Lindsley DH, Dixon SA (1976) Diopside-enstatite equilibria at 850–1,400° C, 5–35 kbar. Am J Sci 276:1285–1301

Melson WG, Hart SR, Thompson G (1972) St. Paul's rocks, equatorial Atlantic: Petrogenesis, radiometric ages, and implications on sea-floor spreading. Geol Soc Am Mem 132:241–272

Melson WG, Jarosewich E, Bowen VT, Thompson G (1967) St. Peter and St. Paul rocks: A high temperature mantle-derived intrusion. Science 155:1532–1535

Merrill RB, Wyllie PJ (1973) Absorption of iron by platinum capsules in high pressure rock melting experiments. Am Mineral 58:16–20

Millhollen GL, Irving AJ, Wyllie PJ (1974) Melting interval of peridotite with 5.7 per cent water to 30 kilobars. J Geol 82:575–587

Mori T, Green DH (1978) Laboratory duplication of phase equilibria observed in natural garnet lherzolites. J Geol 86:83–97

Mysen BO, Boettcher AL (1975) Melting of hydrous mantle. I. Phase relations of natural peridotite at high pressures and temperatures with controlled activities of water, carbon dioxide and hydrogen, and II. Geochemistry of crystals and liquids formed by anatexis of mantle peridotite at high pressures and temperatures as a function of controlled activities of water, hydrogen and carbon dioxide. J Petrol 16:520–548 und 549–592

Nehru CE, Wyllie PJ (1975) Compositions of glasses from St. Paul's peridotite partially melted at 20 kilobars. J Geol 83:455–471

Nicholls IA (1974) Liquids in equilibrium with peridotitic mineral assemblages at high water pressures. Contrib Mineral Petrol 45:289–316

Nicholls IA, Ringwood AE (1973) Effect of water on olivine stability in tholeiites and production of silica-saturated magmas in the island arc environment. J Geol 81:285–300

Perkins III D, Newton RC (1980) The compositions of coexisting pyroxenes and garnet in the system $CaO-MgO-Al_2O_3-SiO_2$ at 900°–1,100° C and high pressures. Contrib Mineral Petrol 75:291–300

Piwinskii AJ (1968a) Studies of batholithic feldspars: Sierra Nevada, California. Contrib Mineral Petrol 17:204–223

Piwinskii AJ (1968b) Experimental studies of igneous rock series, Central Sierra Nevada batholith, California. J Geol 76:548–570

Reed SJB, Ware NG (1975) Quantitative electron microprobe analysis of silicates using energy-dispersive X-ray spectrometry. J Petrol 16:499–519

Ryabchikov ID, Boettcher AL (1980) Experimental evidence at high pressure for potassic metasomatism in the mantle of the earth. Am Mineral 65:915–919

Ryabchikov ID, Schreyer W, Abraham K (1982) Compositions of aqueous fluids in equilibrium with pyroxenes and olivines at mantle pressures and temperatures. Contrib Mineral Petrol 79:80–84

Sekine T, Wyllie PJ, Baker DR (1981) Phase relationships at 30 kbar for quartz eclogite composition in $CaO-MgO-Al_2O_3-SiO_2-H_2O$ with implications for subduction zone magmas. Am Mineral 66:935–950

Sekine T, Wyllie PJ (1982a) Phase relationships in the system $KAlSiO_4-Mg_2SiO_4-SiO_2-H_2O$ as a model for hybridization between hydrous siliceous melts and peridotite. Contrib Mineral Petrol 79:368–374

Sekine T, Wyllie PJ (1982b) Synthetic systems for modelling hybridization between hydrous siliceous magmas and peridotite in subduction zones. J Geol 90:734–741

Stern CR, Wyllie PJ (1978) Phase compositions through crystallization intervals in basalt-andesite-H_2O at 30 kbar with implications for subduction zone magmas. Am Mineral 63:641–663

Stern CR, Wyllie PJ (1981) Phase relationships of I-type granite with H_2O to 35 kilobars: the Dinkey Lakes biotite-granite from the Sierra Nevada batholith. J Geophys Res 86:10412–10422

Wyllie PJ (1979) Magmas and volatile components. Am Mineral 64:469–500

Wyllie PJ (1981) Plate tectonics and magma genesis. Geol Rundsch 70:128–153

Wyllie PJ, Sekine T (1982) The formation of mantle phlogopite in subduction zone hybridization. Contrib Mineral Petrol 79:375–380

Received September 6, 1982; Accepted October 10, 1982